中國機械工程學刊第四十一卷第六期第 699~712 頁(民國一百零九年)
Journal of the Chinese Society of Mechanical Engineers, Vol.41, No.6, pp.699~712 (2020)

Thermal Analysis on Non-Newtonian Nanofluid in Double Tube Heat Exchanger with Staggered Oval Cross-section Pipe as Inner Pipe

Chen-Hsin Lin*, Cha'o-Kuang Chen**and Chieh-Li Chen***

Keywords： heat transfer enhancement; staggered oval tube; tubular heat exchanger; non-Newtonian nanofluids; performance evaluation criterion; synergy angle.

ABSTRACT

In this study, a numerical simulation is used to analyze heat-exchange behaviors of a double tube heat exchanger with a staggered oval cross-section pipe as the inner pipe. In addition, non-Newtonian nanofluid and water are considered to be the working fluid, respectively flowing in the inner tube and outer tube. The non-Newtonian nanofluid is composed of non-Newtonian base fluid and nanoparticle. Besides, a single-phase fluid model was adopted. The purpose of this study is to investigate the heat exchange behavior of non-Newtonian nanofluid concerning different flow behavior index, the inlet velocity and nanoparticle volume fraction. Therefore, the velocity distribution, isotherms contours, synergy angle distribution, the Nusselt number, pressure drop and performance evaluation criterion (PEC) had been studied and calculated. It can be discovered that the heat transfer performance becomes better when the flow behavior index decreases; the inlet velocity of the inner pipe decreases; the inlet velocity of the outer pipe increases and nanoparticle volume fraction decreases.

INTRODUCTION

Due to a rapid improvement of technology, problems of the energy crisis and environmental awareness come out recently. Those problems cause energy cost rising and urge many countries to constitute laws to limit CO_2 emissions. Therefore, engineers start to seek methods to maintain production capacity and reduce cost at the same time, which can maximize production efficiency. Using heat exchangers is one of the common ways to solve the problems stated above in industry concerning thermal-fluid science. To further enhance the efficiency of heat exchangers, two major groups have been exploited, named active and passive techniques. Comparing with active techniques, passive techniques can keep the cost down without additional energy sources. For example, passive techniques include increasing the surface area, adding metal or metal oxide nanoparticles, installing vortex generators and changing the tube structure.

This study is related to the passive techniques and using the staggered oval tube (SOT, also known as alternating elliptical axis tube) as the inner pipe proposed by Guo (2003). Guo indicated that this kind of tube can generate flow vortices, which break the boundary layer, then subsequently, decrease the angle between the temperature gradient and velocity. As a result, the heat transfer performance is promoted with a significant heat transfer raise by comparing with a circular pipe at a comparative small pressure drop for the turbulent flow.

Meng et al. (2005) carried out an experiment and found that the heat transfer of the SOT can be greatly augmented with less increment of flow resistance for Re < 5×10^4. Besides, they mentioned that both the Nusselt number and friction factor of SOT can be correlated with one expression for *Re* ranging from 500 to 5×10^4. Li et al. (2006) made an experimental study on friction factor and the numerical simulation on flow and heat transfer. It revealed that the transition from laminar to turbulent flow occurs at $Re = 1\times10^4$, and the Nusselt number of the SOT is about 84-134% higher than circular tube. Research works also investigated both situations of the SOT in laminar (Chen and Fang, 2004) and turbulent (Chen et al. 2004) flow by numerical simulation. Chen indicated that the axial separation bubbles in the transition section are responsible for the rise of the level of pressure drop. Based on this observation, Chen et al. performed another parametric study (Chen et al., 2006) to search

Paper Received September, 2020. Revised November, 2020. Accepted December, 2020. Author for Correspondence: Cha'o-Kuang Chen

* *Graduate Student, Department of Mechanical Engineering, National Cheng Kung University, Tainan, Taiwan, ROC.*

** *Professor, Department of Mechanical Engineering, National Cheng Kung University, Tainan, Taiwan, ROC.*

*** *Professor, Department of* Aeronautics and Astronautics, *National Cheng Kung University, Tainan, Taiwan, ROC.*

better combinations of geometry parameters, including aspect ratio, length of a section unit and transition section. However, Chen did not find an optimum design to fit all magnitude of Reynolds number. Najafi Khaboshaa and Nazif (2018, 2019) conducted two entropy generation analyses of the SOT in turbulent flow. One is related to the SOT with different angles of pitches, and the other is about using Al_2O_3-water nanofluid with various nanoparticle volume fraction and diameters. The first study showed that the SOT has the best performance at the lowest Reynolds number for the SOT 90°. The other illustrated that the heat transfer of the SOT can be enhanced by using nanofluid. On the other hand, to study the heat transfer performance under a realistic situation, Chen conducted further studies concerning the pipe's performance not only in a cross-flow heat exchanger (Chen, 2007) but also in a parallel or counter flow heat exchanger (Chen and Dung, 2008). In addition, Vaezi et al. (2017) investigated a double tube heat exchanger concerning aspect ratio and Reynolds number in laminar flow. Their works also compared the rate of heat transfer and pressure drop with the circular type, and illustrated a diagram of enhancement ratio (ER) function. In the area of ER > 1, the heat transfer enhancement can be improved with reasonable rise of the pressure drop.

The study concerning the non-Newtonian nanofluid can be divided into two categories. One is discussed the nanofluid with characteristics of non-Newtonian fluid (Kang et al., 2006; Xie et al., 2008). The other is adding nanoparticles into non-Newtonian fluid. Hojatt et al. (2010, 2011) carried out an experimental study to investigate the heat transfer behavior of non-Newtonian nanofluid flowing through a horizontal circular tube with constant wall heat flux in laminar flow. The fluids are made by dispersing γ-Al_2O_3, CuO and TiO_2 nanoparticles in a non-Newtonian fluid (0.5% wt. CMC solution). Hojatt showed that the heat transfer coefficient of non-Newtonian nanofluids are larger than that of the base fluid. Also, the enhancement of the heat transfer coefficient and Nusselt number increase by increasing the nanoparticle volume fraction. Baheri et al. (2014) used CuO and 0.5% wt. CMC non-Newtonian nanofluid as the working fluid, then numerically investigated heat and flow characteristics in 2-D parallel plate microchannel with and without micromixers. The work demonstrated that increasing Reynolds number and nanoparticle volume fraction increase not only the heat transfer but also friction coefficients of non-Newtonian nanofluid. Although nanoparticles enhance the Nusselt number in non-Newtonian base fluid, but this increasing is higher for Newtonian fluid.

In this paper, the main purpose is to study the heat and fluid characteristics of a double tube heat exchanger with a staggered oval cross-section pipe as the inner pipe. Meanwhile, the working fluid of the inner pipe is non-Newtonian nanofluid, which is chosen to compare with the water. This study will discuss three different parameters, including flow behavior index, inlet velocity, and nanoparticle volume fraction. Therefore, streamlines, isotherms contours, pressure drop, Nusselt number and field synergy angle are used to analyze numerical results. Finally, the performance evaluation criterion (PEC) has been adopted to describe the heat transfer efficiency.

MATHEMATICAL FORMULATION

Physical model

A two-dimensional (2-D) geometry of a double tube heat exchanger with a staggered oval cross-section pipe as the inner pipe is represented in Figure 1a. The diameter of the outer circular pipe, D, is 33 mm. The inner pipe is composed of two parts, circular and oval sections. The diameters of the circular part at entrance and exit (d) are both 16.5 mm. On the other hand, the long (d1) and short (d2) diameter of the oval part are 20 mm and 13 mm, respectively. In addition, the length of circular sections (L) and oval sections (A) are 30 mm and 34 mm, respectively. It should be noted that there are several transition sections between each section, whose length (B) is 6 mm. Also, the thickness (t) is 0.5 mm for both pipes considered. The number of double tube sections is 11, and total length is 506 mm. A three-dimensional (3-D) isometric view which is properly cut off is shown in Fig. 1b. As shown, for a counter flow heat exchanger, the flow direction is positive z-direction for the inner pipe, and negative for the outer pipe. To ensure the flow reaching fully developed, the outlet section length has been tested. Both of pipes are made of iron, whose density, specific heat capacity and heat conductivity are 8030 kg m^{-3}, 502.48 J kg^{-1} K^{-1} and 77 Wm^{-1} K^{-1}, respectively.

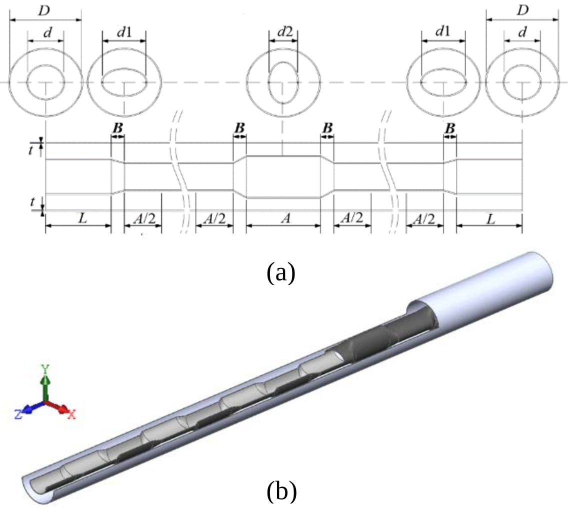

Fig. 1. Geometries of a double tube heat exchanger with a staggered oval cross-section pipe as the inner pipe: (a) 2-D geometrical dimensions and (b) 3-D isometric view.

Working fluid

The fluid inside the outer pipe is water. However, the fluid used in the inner pipe is a mixture of non-Newtonian fluid and nanosized Al_2O_3 particles at nanoparticle volume fraction being 0%, 3% and 5%. By assuming that the nanoparticles are well dispersed within the base fluid, the effective physical properties of the mixture can be evaluated by using some classical single-phase formulas (Lamraoui et al., 2019). To compute density, specific heat capacity, viscosity and thermal conductivity, a couple of equations from (1) to (4) have been applied (Mahian et al., 2013). The physical and thermal properties of the considered working fluid are listed in Table 1.

$$\rho_{\mathrm{nf}} = (1-\phi)\rho_{\mathrm{bf}} + \phi\rho_{\mathrm{p}}, \tag{1}$$

$$\mathrm{C}_{\mathrm{nf}} = \frac{(1-\phi)\rho_{\mathrm{bf}}\mathrm{C}_{\mathrm{bf}} + \phi\rho_{\mathrm{p}}\mathrm{C}_{\mathrm{p}}}{\rho_{\mathrm{nf}}}, \tag{2}$$

$$\frac{\mu_{\mathrm{nf}}}{\mu_{\mathrm{bf}}} = \frac{1}{(1-\phi)^{2.5}}, \tag{3}$$

$$\frac{k_{\mathrm{nf}}}{k_{\mathrm{bf}}} = 4.97\phi^2 + 2.72\phi + 1. \tag{4}$$

Table 1. The value of Physical and thermal properties of nanofluid used.

ϕ (%)	ρ_{nf} (kg m^{-3})	μ_{nf} (kg m^{-1} s^{-1})	C_{nf} (J kg^{-1} K^{-1})	k_{nf} (W m^{-1} K^{-1})
0	998.2	0.001003	4182	0.6
3	1087.65	0.0010824	3827.748	0.65164
5	1147.29	0.0011402	3622.270	0.68906

Governing equations

In this research, due to a condition of turbulent flow, 3-D Reynolds-averaged Navier-Stokes (RANS) equations are adopted. Also, to solve the closure problem of turbulence, the SST k-ω turbulence model mentioned by Menter (1994) was applied to complement insufficient equations. Combing these two parts, under assumptions of steady state, incompressible flow and constant material properties, the governing equations can be written as follows.

Continuity equation:

$$\frac{\partial \bar{u}_i}{\partial x_i} = \frac{\partial u_i'}{\partial x_i} = 0 \tag{5}$$

Momentum equation:

$$\rho_{\mathrm{nf}}\bar{u}_j \cdot \frac{\partial \bar{u}_i}{\partial x_j} = -\frac{\partial \bar{P}}{\partial x_i} + \frac{\partial}{\partial x_j}(\bar{\tau}_{ij} - \rho_{\mathrm{nf}}\overline{u_i'u_j'}), \tag{6}$$

For non-Newtonian nanofluid, it should be noted that

$$\bar{\tau}_{ij} = \mu_{\mathrm{nf}}\frac{\partial}{\partial x_j}(\frac{\partial \bar{u}_i}{\partial x_j} + \frac{\partial \bar{u}_j}{\partial x_i}),\quad \mu_{\mathrm{nf}} = \mathrm{K}\,\dot{\gamma}^{n-1} = \mathrm{K}(\frac{\partial \bar{u}_i}{\partial x_j} + \frac{\partial \bar{u}_j}{\partial x_i})^{n-1} \tag{7}$$

where viscosity of the non-Newtonian nanofluid (μ_{nf}) will change along with rate of shear strain ($\dot{\gamma}$). In Eq. (7), K represents a flow consistency index, and n is flow behavior index.

On the other hand, the equations are written in a form of Einstein notation with lower indices "i" or "j". Both range over a set {1, 2, 3}, which is equivalent to coordinate axes {x, y, z} in the following equations.

Energy equation:

For fluid,

$$\rho_{\mathrm{nf}}\mathrm{C}_{\mathrm{nf}} \cdot \bar{u}_j \frac{\partial \bar{T}}{\partial x_j} = \frac{\partial}{\partial x_j}(k_{\mathrm{nf}}\frac{\partial \bar{T}}{\partial x_j} - \rho_{\mathrm{nf}}\mathrm{C}_{\mathrm{nf}}\overline{u_j'T'} + \bar{u}_i\bar{\tau}_{ij}), \tag{8}$$

For solid:

$$k_{\mathrm{s}}\frac{\partial^2 T}{\partial x_j \partial x_j} = 0. \tag{9}$$

Turbulent kinetic energy k (m^2 s^{-2}) transport equation:

$$\rho\frac{\partial}{\partial x_i}(\mathrm{k}\,u_i) = \frac{\partial}{\partial x_j}\left[\left(\mu + \frac{\mu_t}{\sigma_{\mathrm{k}}}\right)\frac{\partial \mathrm{k}}{\partial x_j}\right] + \tilde{G}_{\mathrm{k}} - \rho\beta^*\mathrm{k}\,\omega. \tag{10}$$

Specific dissipation rate ω (s^{-1}) transport equation:

$$\rho\frac{\partial}{\partial x_i}(\omega u_i) = \frac{\partial}{\partial x_j}\left[\left(\mu + \frac{\mu_t}{\sigma_\omega}\right)\frac{\partial \omega}{\partial x_j}\right] + G_\omega - \rho\beta\omega^2 + 2(1-F_1)\rho\sigma_{\omega,2}\frac{1}{\omega}\frac{\partial \mathrm{k}}{\partial x_j}\frac{\partial \omega}{\partial x_j}. \tag{11}$$

In Eq. (10) and (11), the left-hand side are related to the transport of k or ω by convection respectively. On the other side, according to the order, the three terms denote the transport of k or ω by diffusion, the generation of k or ω and the dissipation of k or ω. Unlike Eq. (10), the last term in Eq. (11) represents the cross-diffusion, which is caused by a transformation of a ε equation into an ω equation.

Further details about the SST k-ω turbulence model and all related functions and constants in Eq. (10) and (11) can refer to the work by Menter (1993).

Boundary conditions

To simplify the calculation process, the model is symmetrically cut into four parts. One of them is set to be the zone of simulation. Meanwhile, symmetry boundary conditions are applied to the XZ and YZ plane of it. Those are

$$\frac{\partial T}{\partial n}=0\ ,\ \frac{\partial V}{\partial n}=0\ , \tag{12}$$

where n represents the direction normal to the XZ and YZ plane.

On the fluid/solid interfaces, in order to maintain continuity, the boundary conditions are:

$$T_{\mathrm{s}}=T_{\mathrm{f}}\ ,\ k_{\mathrm{s}}\frac{\partial T_{\mathrm{s}}}{\partial n}=k_{\mathrm{f}}\frac{\partial T_{\mathrm{f}}}{\partial n}\ ,\ V=0\ , \tag{13}$$

where the subscripts "s" and "f" denote solid and fluid, respectively. Besides, a no-slip boundary condition is applied.

For the inner pipe, the boundary conditions are as follows.

At inlet:

$$T=T_{\mathrm{i}}=293\mathrm{K}\ ,\ w=w_{\mathrm{i}}\ ,\ u=v=0\ . \tag{14}$$

At outlet:

$$\frac{\partial T}{\partial z}=0\ ,\ \frac{\partial u}{\partial z}=\frac{\partial v}{\partial z}=\frac{\partial w}{\partial z}=0\ ,\ P=P_{\mathrm{atm}}\ . \tag{15}$$

The temperature and velocity gradient in flow direction is zero, and the pressure is also assumed equal to 1 atm (atmospheric pressure). Moreover, these conditions are the same as the boundary conditions at the outlet of the outer pipe.

Boundary conditions for the outer pipe are described as the following.

At inlet:

$$T=T_{\mathrm{o}}=363\mathrm{K}\ ,\ w=w_{\mathrm{o}}\ ,\ u=v=0\ . \tag{16}$$

At outlet:

$$\frac{\partial T}{\partial z}=0\ ,\ \frac{\partial u}{\partial z}=\frac{\partial v}{\partial z}=\frac{\partial w}{\partial z}=0\ ,\ P=P_{\mathrm{atm}}\ . \tag{17}$$

For the outer pipe wall, due to an adiabatic condition is applied to it, temperature gradient in the wall normal direction should be zero.

$$\frac{\partial T}{\partial n}=0\ . \tag{18}$$

Data processing

Because the working fluid flowing in the inner pipe is different from the outer one, the relationship between Reynolds number and inlet velocity is listed below.

Inner pipe:

$$Re_{\mathrm{nf}}=\frac{\rho_{\mathrm{nf}}\bar{w}_{\mathrm{i}}^{\,2-n}d^{\,n}}{\mu_{\mathrm{nf}}}\ . \tag{19}$$

Outer pipe:

$$Re=\frac{\rho\bar{w}_{\mathrm{o}}D_h}{\mu}\ . \tag{20}$$

In order to calculate the diameter of an annulus (entrance shape of the outer pipe), a hydraulic diameter is adopted. In the Eq. (20), D_h represents the hydraulic diameter, which is defined as

$$D_h=\frac{4\mathrm{A}}{\mathrm{P}}\ , \tag{21}$$

where A is the cross-section inlet area of the outer pipe, and P is the wetted perimeter of the cross-section of the outer pipe. To calculate the Nusselt number, which is defined as

$$Nu=\frac{h\,\mathrm{L}}{k}\ . \tag{22}$$

For the averaged Nusselt number of the heat exchanger, it can be evaluated by

$$\overline{Nu}=h_{\mathrm{avg}}\frac{\mathrm{L}}{k}=\frac{q''_w}{\Delta T_m}\frac{D_h}{k}\ , \tag{23}$$

where ΔT_m is a so-called logarithmic mean temperature difference (LMTD). Under the situation of counter flow, it is defined by the logarithmic mean as follows:

$$\Delta T_m=\frac{\Delta T_1-\Delta T_2}{\ln(\dfrac{\Delta T_1}{\Delta T_2})}=\frac{(T_{\mathrm{hi}}-T_{\mathrm{co}})-(T_{\mathrm{ho}}-T_{\mathrm{ci}})}{\ln(\dfrac{T_{\mathrm{hi}}-T_{\mathrm{co}}}{T_{\mathrm{ho}}-T_{\mathrm{ci}}})}\ . \tag{24}$$

To assess heat transfer performance, the performance evaluation criterion (PEC), which was developed by Webb and Kim (2005) is used in this paper. The PEC can be evaluated by the following function.

$$\mathrm{PEC}=\frac{\overline{Nu}\big/\overline{Nu_0}}{(f\big/f_0)^{1/3}}\ , \tag{25}$$

where $\overline{Nu_0}$ and f_0 are acquired by using water as the working fluid with same inlet velocity and temperature.

GRID INDEPENDENCE AND MODEL VALIDATION

In this simulation, the grids are generated by the sweep method. To ensure that the numerical results will not be affected by the number of grids, a grid independent test has been done. The inlet velocity of the inner pipe is set at 0.23814 m/s based on the parameters of ϕ = 3%, n = 0.5 and Re_{nf} = 15000. For the outer pipe, it is set at 0.97239 m/s corresponding to Re = 15000. To achieve an appropriate grid number, friction factor is tested with four different 3-D grid number. From Table 2, it can be seen that the difference of friction factor between grid number 1,599,455 and 2,388,946 is only 0.00027, which is small enough and means that grid number of 1,599,455 is sufficient to achieve grid independence, therefore, it will be applied for the following numerical study.

In order to validate reliability of the numerical simulation results, friction factor of the inner pipe was selected to test. However, there are no experimental or numerical data about the heat exchange of staggered oval pipe by considering non-Newtonian nanofluid as the working fluid. Therefore, the validated part in this

Table 2. Grid independence test in terms of friction factor.

Grid number	f	δf
1,308,656	0.04353	-
1,407,624	0.04314	0.00039
1,599,455	0.04268	0.00046
2,388,946	0.04241	0.00027

study is conducted by comparison with the experimental and numerical results given by Meng et al. (2005) and Chen et al. (2004), respectively, for a case of water as the working fluid. Experimental results of Meng et al. (2005) revealed that friction factor can be correlated by one expression with Reynolds number ranging from 500 to 50000. The correlation is

$$f = 1.54Re^{-0.32}. \quad (26)$$

On the other hand, for the present study and numerical results given by Chen et al. (2004), friction factor can be calculated by Darcy-Weisbach equation

$$f = \frac{\Delta P}{\frac{1}{2}\rho \mathrm{U}_{avg}^2}\frac{\mathrm{D}}{\mathrm{L}_t}, \quad (27)$$

where ΔP is the pressure drop over the inlet and outlet along the pipe, U_{avg} is the average velocity inside the pipe, L_t is the total length of the pipe and D is the diameter of the inlet. As shown in Figure 2, comparing with the other two data, the maximum errors of friction factor are less than 5%, which represents that the present calculation is in good agreement with the experimental fitted curve and the numerical results.

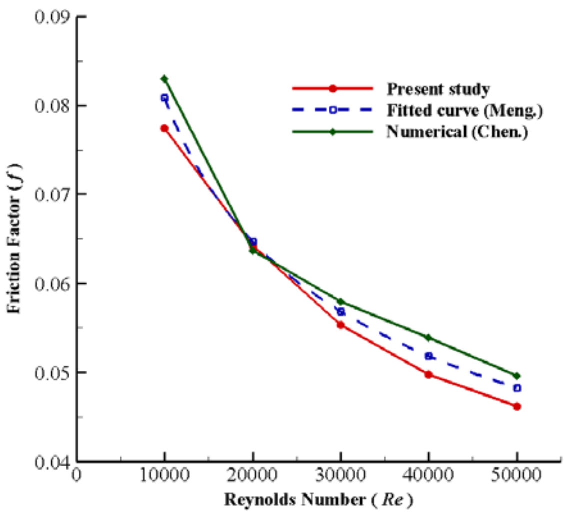

Fig. 2. Validation test by comparing results of friction factor in present study with numerical results by Chen et al. (2004) and an experimental fitted curve by Meng. (2005)

RESULT AND DISCUSSION

In this section, the iwnvestigation is focus on three parameters about non-Newtonian nanofluid as the working fluid. Those are flow behavior index (n), the inlet velocity of the inner and outer pipe ($\bar{w}_i$ and $\bar{w}_o$), and nanoparticle volume fraction (ϕ). In every section, flow field and heat transfer characteristics will be discussed. Furthermore, performance evaluation criterion and synergy angle distribution contours will be used to assess the performance.

Effect of flow behavior index (n)

To investigate the influences caused by n, the value of ϕ, $\bar{w}_i$ and $\bar{w}_o$ are fixed at 3%, 0.23814 m/s (Re_{nf} = 15000) and 0.97239 m/s (Re = 15000), respectively, for the value of n = 0.5, 0.7, 1, 1.3 and 1.5. Figure 3 displays the surface streamlines of the double pipe heat exchanger at 0.373 m under different n. It can be observed that those streamlines form into several axial vortices not only in the inner pipe but also in the outer pipe. These vortices are also known as secondary flow, which intensifies fluid mixing and destroys the boundary layer. As can be observed, there are eight vortices when n = 0.5, 0.7 and 1. Also, the streamlines are centralized with the decreasing of n. In addition, the number of vortices will become four while n > 1.

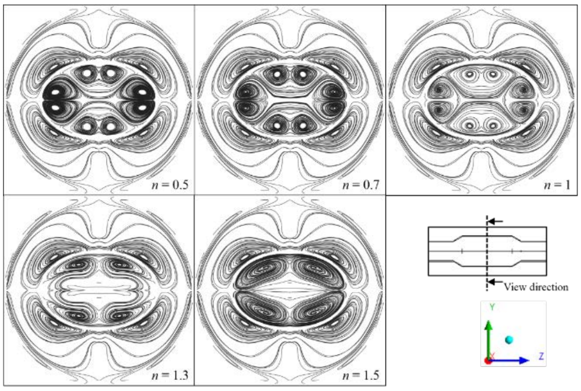

Fig. 3. Surface streamlines at 0.373 m under different flow behavior index.

Figure 4 shows the velocity distribution and 3-D streamlines in the inner pipe from 0.313 m to 0.373 m under different n. It can be found that the velocity distribution in every section display a "X" shape when $n \leq 1$. However, when $n > 1$, the shape of velocity distribution will gradually become "concentric circles" form. In addition, for n = 1.5, the streamlines almost concentrate at the center comparing to other value of n. Also, it can be noticed that the center velocity is getting larger with a rising of n.

The isotherms in Figure 5 present the temperature distribution at 0.373 m under different n. Due to the effects of secondary flow, the flow with high

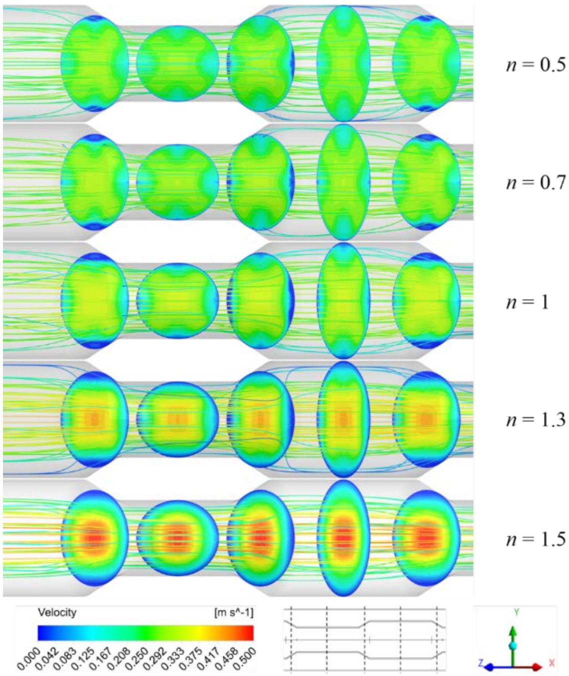

Fig. 4. 3-D streamlines and velocity distribution from 0.313 m to 0.373 m under different flow behavior index.

temperature can be taken to the inner pipe wall and promotes heat transfer. Therefore, the temperature has a remarkable decrease along both axes of the oval section. Comparing to Fig. 3 and Fig. 4, the temperature distribution is similar to the velocity distribution, and the main region for heat transfer is corresponding to the space between vortices.

Figure 6 is the results about the synergy angle distribution at 0.373 m under different *n*. In the synergy angle analysis, the primary target is to improve the synergy between the velocity and temperature gradient for enhancing heat transfer. Namely, heat transfer can be enhanced when synergy angle closes to 0° or 180°. In the following discussion, if the value of synergy angle is greater than 90°, its complementary angle will be taken. As shown in Fig.

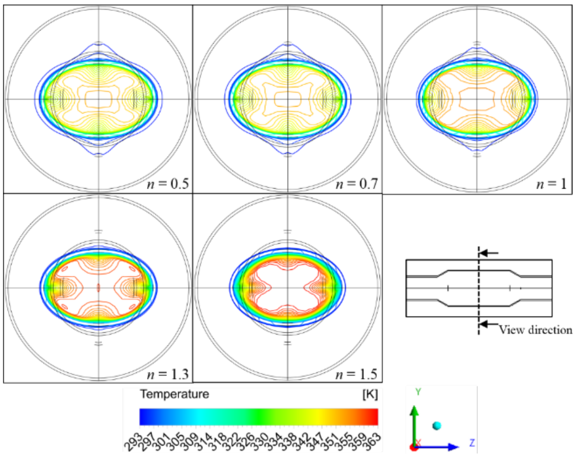

Fig. 5. Temperature distribution at 0.373 m under different flow behavior index.

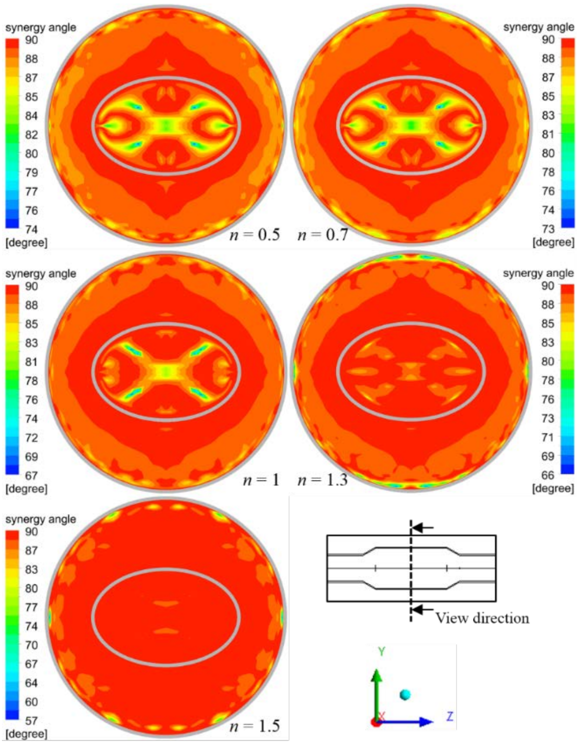

Fig. 6. Synergy angle distribution at 0.373 m under different flow behavior index.

6, for the outer pipe, it is obvious that many places of synergy angle are almost or exactly 90°. The synergy angle is diversified and has a remarkable change with the increasing of *n* for inner pipe. The main reason is that the secondary flow influences the angle between velocity direction and temperature gradient. For n > 1, the values of synergy angle are in general closer to 90° than those of n < 1. In other words, a smaller value of *n* can lead to a better heat transfer efficiency.

Figure 7 gives the average Nusselt number ($\overline{Nu}$) of the double tube heat exchanger with different *n* and $\bar{w}_{\mathrm{i}}$. On one hand, an increasing of $\bar{w}_{\mathrm{i}}$ will lead to a larger $\overline{Nu}$. On the other hand, a decreasing of *n* can also raise $\overline{Nu}$. The difference between them is that changing the value of *n* is much more helpful for improving heat transfer than increasing $\bar{w}_{\mathrm{i}}$. Figure 8 illustrates the average Nusselt number ratio of non-Newtonian nanofluid to water versus $\bar{w}_{\mathrm{i}}$ under different flow behavior index. Although *n* = 0.5 can mostly enhance $\overline{Nu}$, the increasing level of it will gradually decrease if $\bar{w}_{\mathrm{i}}$ increases. $\overline{Nu}$ for non-Newtonian nanofluid with $\bar{w}_{\mathrm{i}}$ = 0.11449 m/s, 0.18173 m/s and 0.23814 m/s are 1.94, 1.69 and 1.56 times the value of water, respectively.

Figure 9 shows the pressure drop (ΔP) of the inner pipe with different *n* and $\bar{w}_{\mathrm{i}}$. It shows that ΔP is

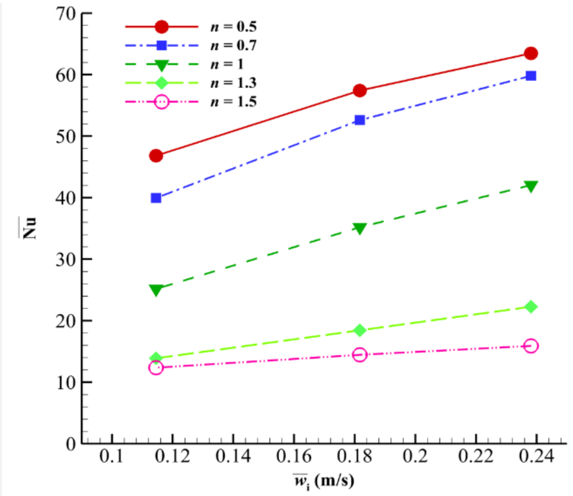

Fig. 8. Distribution of average Nusselt number versus $\bar{w}_i$ under different flow behavior index.

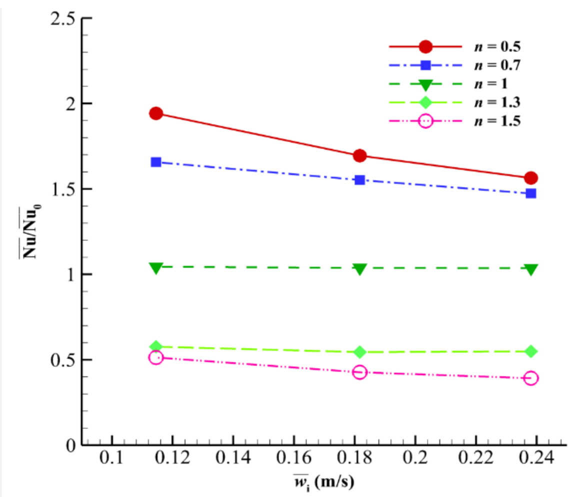

Fig. 7. Average Nusselt number ratio of non-Newtonian nanofluid to water versus $\bar{w}_i$ under different flow behavior index.

rising as $\bar{w}_i$ increases. Also, the increasing level of ΔP becomes larger as n gets larger. Comparing the case of non-Newtonian nanofluid as the working fluid to water at the same $\bar{w}_i$ shown in Figure 10, the ΔP ratio of non-Newtonian nanofluid to water may exceed one, for $n \geq 1$, which means that it needs more power to force non-Newtonian nanofluid than water. Nevertheless, for $n < 1$, the ratio will fall below one. Besides, the ratio slightly decreases with the increasing of $\bar{w}_i$ for the cases of n = 0.5, 1.3 and 1.5. For n = 0.5, the ΔP ratio is 0.61, 0.55 and 0.52 with $\bar{w}_i$ = 0.11449 m/s, 0.18173 m/s and 0.23814 m/s, respectively.

In Figure 11, the variation of the PEC with different n and $\bar{w}_i$ is presented. For n = 0.5, 0.7 and 1.5, the PEC decreases with the decreasing of $\bar{w}_i$.

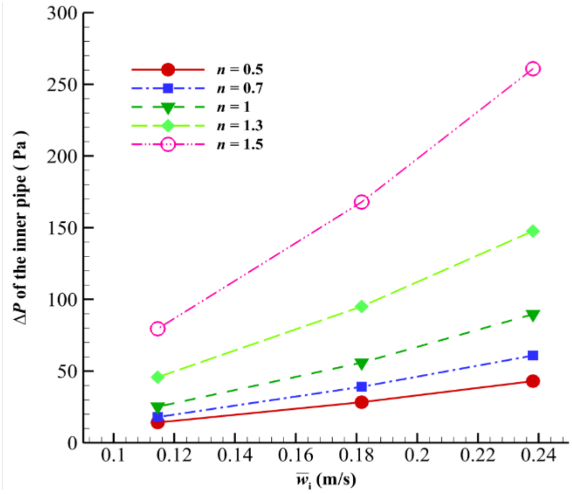

Fig. 9. Distribution of pressure drop versus $\bar{w}_i$ under different flow behavior index.

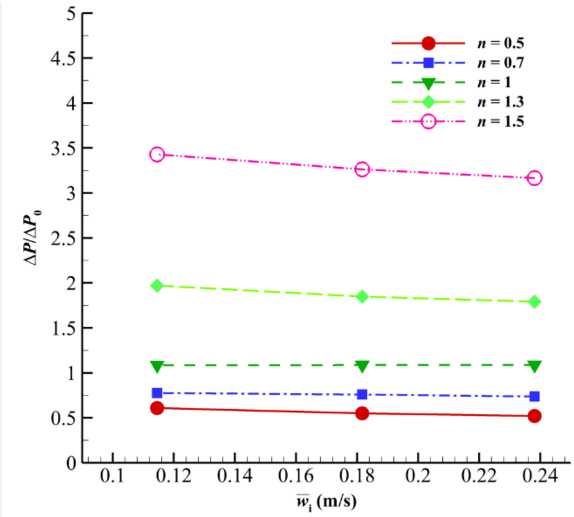

Fig. 10. Pressure drop ratio of non-Newtonian nanofluid to water versus $\bar{w}_i$ under different flow behavior index.

Also, they have the maximum value of the PEC at $\bar{w}_i$ = 0.11449 m/s. On the other hand, the PEC does not vary significantly with respect to $\bar{w}_i$ for n = 1 and 1.3. The highest value of the PEC (2.29) will be found at n = 0.5 and $\bar{w}_i$ = 0.11449 m/s, which demonstrates that using non-Newtonian nanofluid with a small value of n will have significant advantages than using water as the working fluid.

Effect of the inlet velocity ($\bar{w}_i$ and $\bar{w}_o$)

To study the influences of the inlet velocity of the outer pipe ($\bar{w}_o$), the value of n, ϕ and $\bar{w}_i$ are respectively fixed to 0.5, 3% and 0.23814 m/s (Re_{nf} = 15000). Meanwhile, the value of $\bar{w}_o$ will be discussed at 0.32413 m/s, 0.64826 m/s and 0.97239

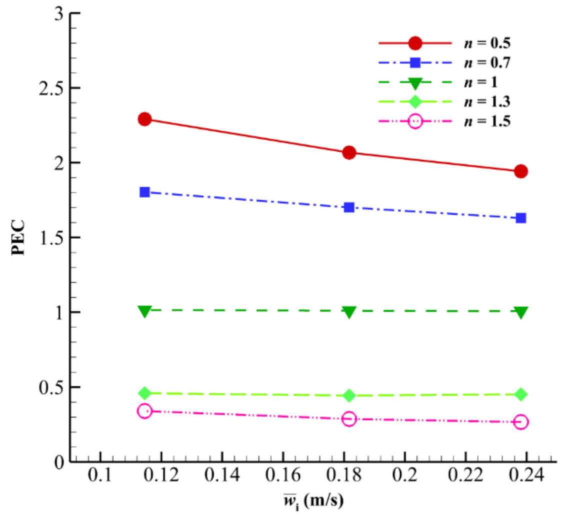

Fig. 11. The Performance evaluation criterion as a function of $\bar{w}_i$ under different flow behavior index.

m/s, corresponding to Re = 5000, 10000 and 15000, respectively. Figure 12 shows the surface streamlines at 0.373 m under a change of $\bar{w}_o$. The main difference between these figures is the location of vortices in the inner pipe. For $\bar{w}_o$ = 0.32413 m/s and 0.64826 m/s, the vortices appear near the upper and lower middle. Then, the vortices not only move to their left-hand or right-hand side but also become larger at $\bar{w}_o$ = 0.97239 m/s. In addition, because $\bar{w}_i$ does not change, the surface streamlines in the section of the inner pipe almost remains the same with an increasing of $\bar{w}_o$.

Figure 13 displays the velocity distribution and 3-D streamlines in the outer pipe from 0.313 m to 0.373 m with different $\bar{w}_o$. With the increasing of $\bar{w}_o$, the maximum velocity of the outer pipe increases proportionally to $\bar{w}_o$. Besides, the velocity distribution around the section of the inner pipe at $\bar{w}_o$ = 0.97239 m/s is different from the others. Such as the section at 0.373 m, its variation of velocity at the upper and lower middle is more concentrated on the middle than that of $\bar{w}_o$ = 0.32413 m/s and 0.64826 m/s.

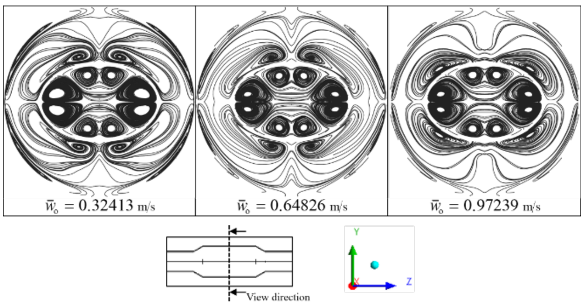

Fig. 12. Surface streamlines at 0.373 m under different $\bar{w}_o$.

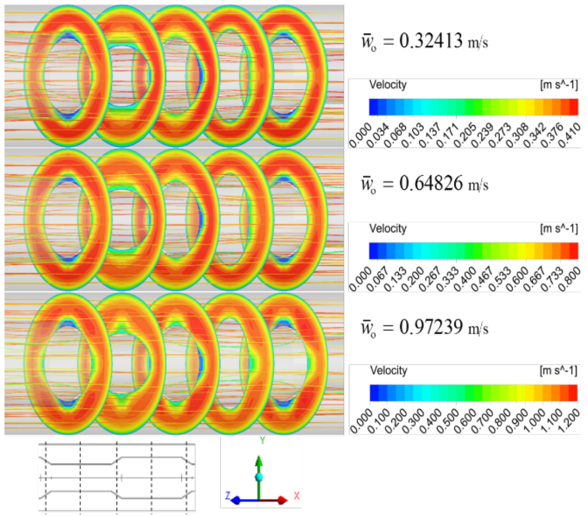

Fig. 13. 3-D streamlines and velocity distribution from 0.313 m to 0.373 m under different $\bar{w}_o$.

Figure 14 presents the isotherms contours of temperature distribution at 0.373 m under different $\bar{w}_o$. Because the location of vortices in the outer pipe are different from each $\bar{w}_o$, the velocity gradient around the inner pipe will be changed and lead to the variation of temperature distribution as shown in Fig. 14. At $\bar{w}_o$ = 0.97239 m/s, not only does the number of isotherms decrease, but the isotherm representing the lowest temperature also concentrates on the middle, which is similar to the velocity distribution at 0.373 m in Fig. 12. It reveals that the secondary flow plays an important role in heat transfer.

The synergy angle distribution at 0.373 m under different $\bar{w}_o$ is shown in Figure 15. According to the figure, raising the value of $\bar{w}_o$ can improve most of synergy angles in the outer pipe. However, decreasing the value of $\bar{w}_o$ can lower the synergy angle around the inner pipe, especially at the place near upper and lower middle.

Figure 16 illustrates the change of average Nusselt number ($\overline{Nu}$) of the double tube heat exchanger under different $\bar{w}_o$ and $\bar{w}_i$. It can be

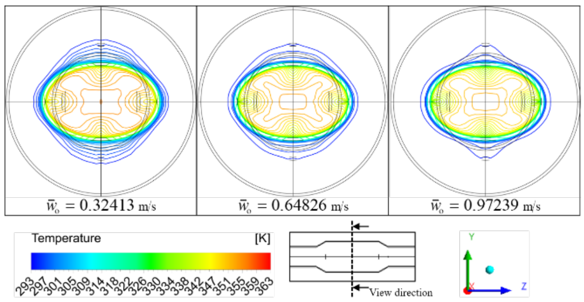

Fig. 14. Temperature distribution at 0.373 m under different $\bar{w}_o$.

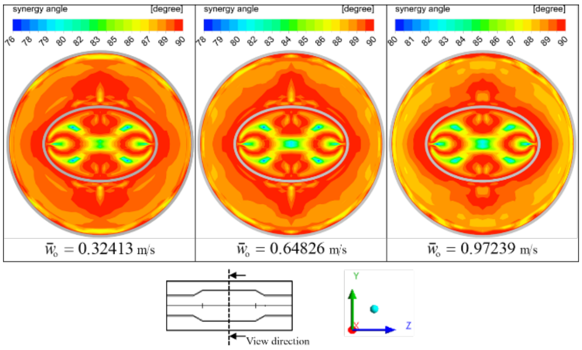

Fig. 16. Synergy angle distribution at 0.373 m under different $\bar{w}_o$.

noticed that $\overline{Nu}$ raises with the increasing of $\bar{w}_i$. Besides, as $\bar{w}_i$ increases, $\overline{Nu}$ can be further enhanced when $\bar{w}_o$ becomes larger. To compare the results with water as the working fluid under the same $\bar{w}_o$ and $\bar{w}_i$, the $\overline{Nu}$ ratio of using non-Newtonian nanofluid to water is shown in Figure 17. It can be found that a better $\overline{Nu}$ can be obtained for $\bar{w}_i$ = 0.11449 m/s.

For $\bar{w}_i$ = 0.11449 m/s, $\overline{Nu}$ obtained using non-Newtonian nanofluid is 1.69, 1.86 and 1.94 times of those using water with $\bar{w}_o$ = 0.32413 m/s, 0.64826 m/s and 0.97239 m/s, respectively. On the other hand, at $\bar{w}_o$ = 0.97239 m/s, $\overline{Nu}$ will increase 1.94, 1.69 and 1.56 times of those using water with $\bar{w}_i$ = 0.11449 m/s, 0.18173 m/s and 0.23814 m/s, respectively.

Figure 18 illustrates the relation of PEC to $\bar{w}_o$ and $\bar{w}_i$. Because the pressure drop in the inner pipe does not change, the curves of the PEC are similar to the result in Fig. 17. Fig. 18 shows that the PEC in all

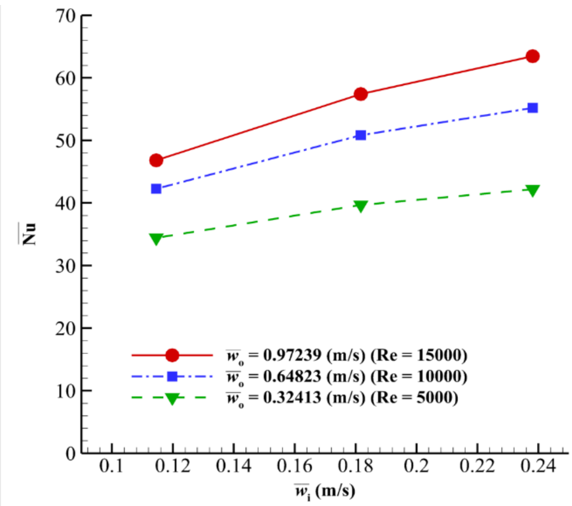

Fig. 17. Distribution of average Nusselt number versus $\bar{w}_i$ with different $\bar{w}_o$.

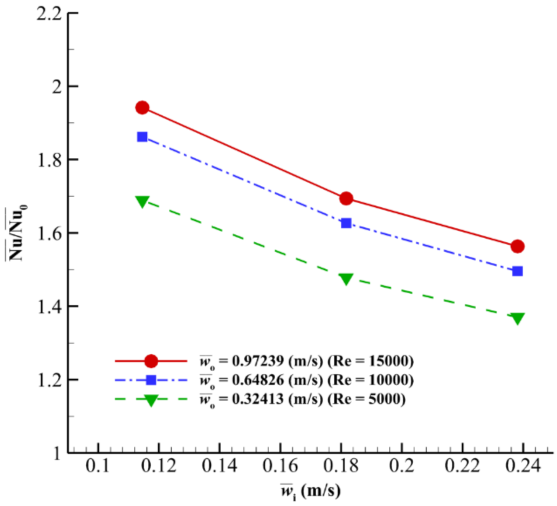

Fig. 15. Average Nusselt number ratio of non-Newtonian nanofluid to water versus $\bar{w}_i$ under different $\bar{w}_o$.

cases are larger than one due to the effect of using non-Newtonian nanofluid. However, the PEC will decrease with the decreasing of $\bar{w}_o$. The largest PEC value of 2.29 can be observed with $\bar{w}_o$ = 0.97239 m/s and $\bar{w}_i$ = 0.11449 m/s. It shows that the heat transfer performance of non-Newtonian nanofluid (n = 0.5) can be improved by raising $\bar{w}_o$.

Effect of nanoparticle volume fraction (ϕ)

In this section, the influences of nanoparticle volume fraction (ϕ) was studied. Therefore, the value of n, $\bar{w}_i$ and $\bar{w}_o$ are respectively fixed at 0.5, 0.23814 m/s (Re_{nf} = 15000) and 0.97239 m/s (Re = 15000). The effect of ϕ is investigated at the value of 0%, 3% and 5%. Figure 19 to Figure 22 display the surface streamlines, velocity distribution, 3-D streamlines, temperature distribution and synergy

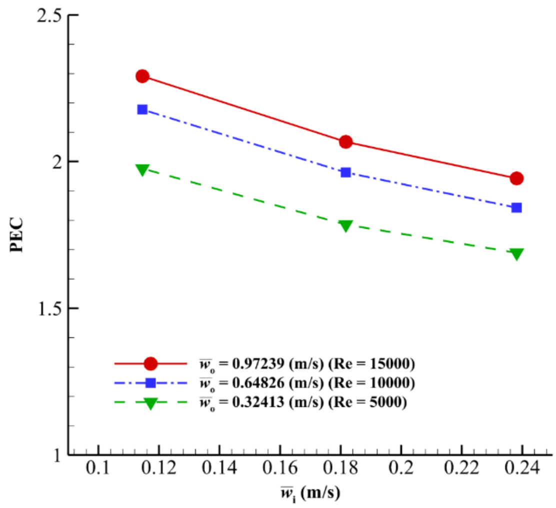

Fig. 18. The Performance evaluation criterion as a function of $\bar{w}_i$ under different $\bar{w}_o$.

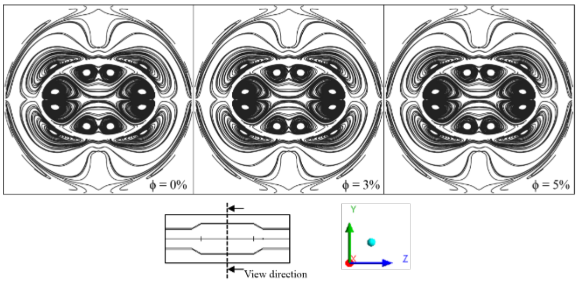

Fig. 19. Surface streamlines at 0.373 m with different nanoparticle volume fraction.

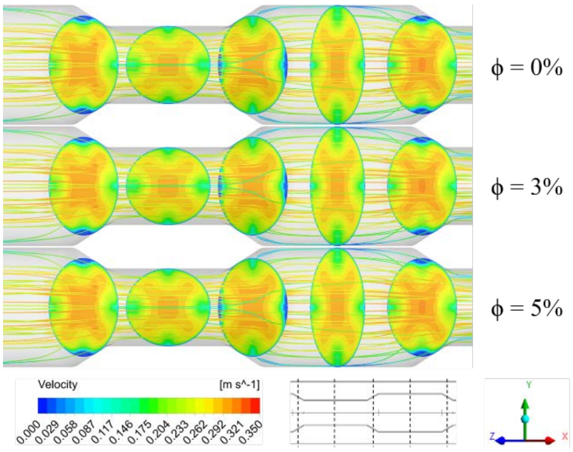

Fig. 21. 3-D streamlines and velocity distribution from 0.313 m to 0.373 m with different nanoparticle volume fraction.

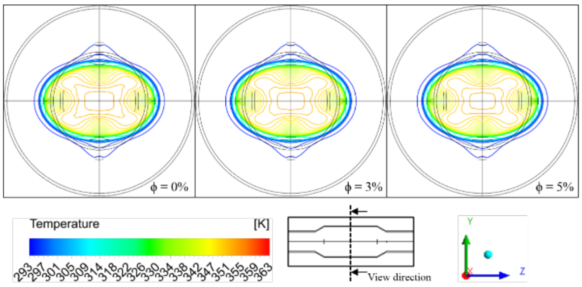

Fig. 22. Temperature distribution at 0.373 m with different nanoparticle volume fraction.

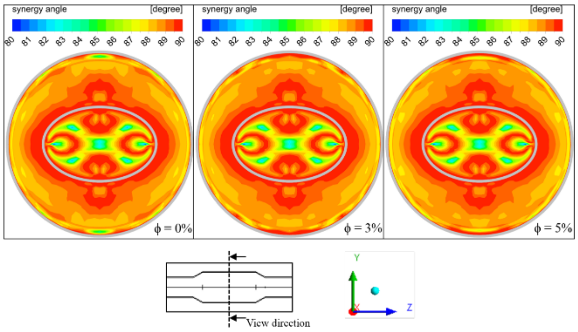

Fig. 23. Synergy angle distribution at 0.373 m with different nanoparticle volume fraction.

angle distribution at same cross section location which have been discussed above. Though there is no significant difference due to a change of ϕ, the variation can still be found by $\overline{Nu}$ and ΔP as follows.

Figure 23 shows the average Nusselt number ($\overline{Nu}$) of the double tube heat exchanger with different ϕ and $\bar{w}_{\mathrm{i}}$. It reveals that $\overline{Nu}$ increases with the increasing of $\bar{w}_{\mathrm{i}}$ owing to the velocity enhancement. Also, $\overline{Nu}$ can be enhanced by increasing the value of ϕ. This is because adding nanoparticles can enhance the thermal conductivity, and improve heat transfer consequently. Figure 24 presents the $\overline{Nu}$ ratio of using non-Newtonian nanofluid to water as the working fluid. According to the result, $\overline{Nu}$ will increase in general at ϕ = 5%, however, comparing with the other two values of ϕ, increasing ϕ does not result a significant change of $\overline{Nu}$.

Figure 25 illustrates the pressure drop (ΔP) of the inner pipe with different ϕ and $\bar{w}_{\mathrm{i}}$. ΔP increases with the increasing of $\bar{w}_{\mathrm{i}}$ and ϕ. As $\bar{w}_{\mathrm{i}}$ increasing, ΔP would be raised with a higher value of ϕ. Figure 26 shows the ΔP ratio of using non-Newtonian nanofluid to water. In general, adding nanoparticles into the working fluid will lead to an increase of ΔP. However, the increase ΔP due to a higher $\bar{w}_{\mathrm{i}}$ will slightly reduce for using non-Newtonian nanofluid than water.

Figure 27 shows the variation of the PEC with different ϕ and $\bar{w}_{\mathrm{i}}$. It can be found that all the values of the PEC are higher than one, but no significant differences in. On the other hand, the PEC reaches its maximum value of 2.29 at ϕ = 0% and $\bar{w}_{\mathrm{i}}$ = 0.11449 m/s, which indicates that higher ϕ would not necessarily enhance the PEC.

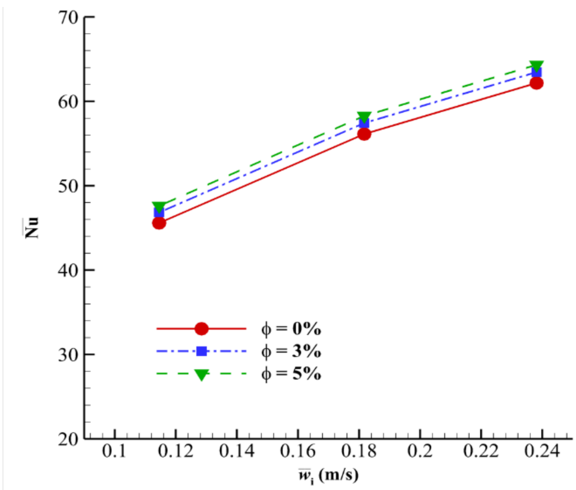

Fig. 20. Distribution of average Nusselt number versus $\bar{w}_{\mathrm{i}}$ under different nanoparticle volume fraction.

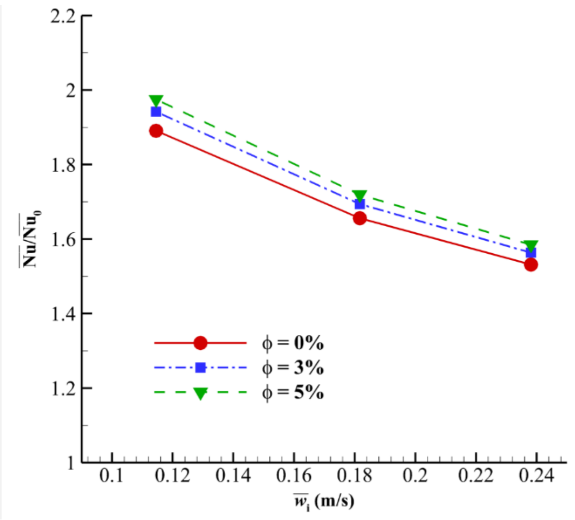

Fig. 25. Average Nusselt number ratio of non-Newtonian nanofluid to water versus $\overline{w}_i$ under different nanoparticle volume fraction.

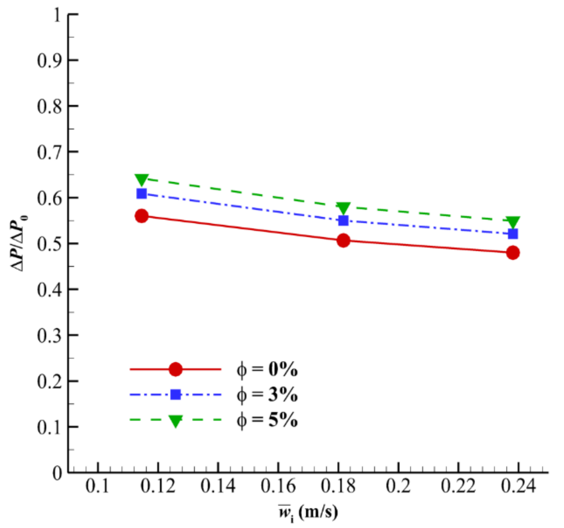

Fig. 27. Pressure drop ratio of non-Newtonian nanofluid to water versus $\overline{w}_i$ under different nanoparticle volume fraction.

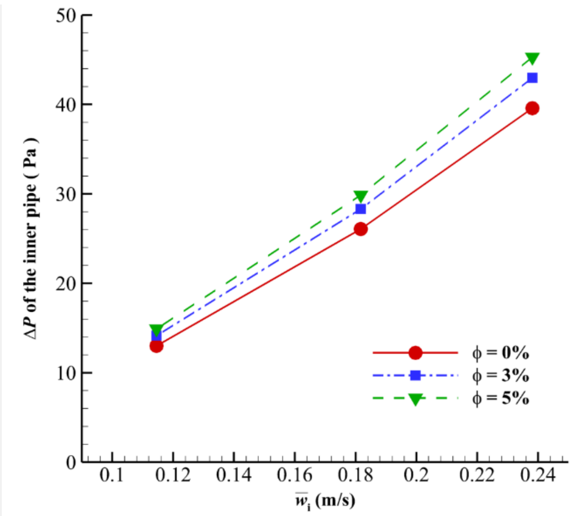

Fig. 26. Distribution of pressure drop versus $\overline{w}_i$ under different nanoparticle volume fraction.

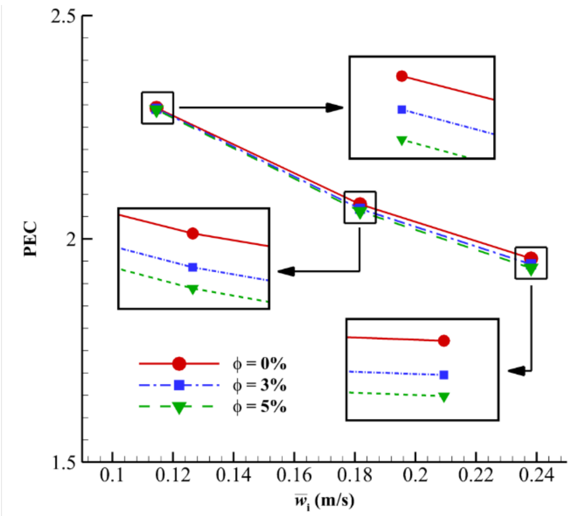

Fig. 24. The Performance evaluation criterion as a function of $\overline{w}_i$ under different nanoparticle volume fraction.

CONCLUSIONS

In this paper, a numerical study was performed to investigate the flow and heat transfer characteristics of the turbulent flow of non-Newtonian nanofluid in a double tube heat exchanger with a staggered oval cross-section pipe as the inner pipe. The influences of the flow behavior index (n), the inlet velocity of the outer and inner pipe ($\overline{w}_o$ and $\overline{w}_i$) and the nanoparticle volume fraction (ϕ) were discussed in this paper. The conclusion remarks are summarized as follows:

1. Due to a staggered oval-cross-section pipe as the inner pipe, several vortices which enhance the heat transfer are generated in the inner and outer pipe. Comparing with water, when non-Newtonian nanofluid (n = 0.5, ϕ = 3%, $\overline{w}_o$ = 0.97239 m/s) is used as the working fluid in the inner pipe, it can be found that the pressure drop will reduce 39-48% from $\overline{w}_i$ = 0.11449 m/s to 0.23814 m/s. However, the heat transfer will improve 56-94% when $\overline{w}_i$ decreases from 0.23814 m/s to 0.11449 m/s. Furthermore, the pressure drop increases and the average Nusselt number decreases with the increasing of n. In this group, the performance evaluation criterion (PEC) shows that n = 0.5 has better performance among the others.
2. Varying the magnitude of $\overline{w}_o$ and $\overline{w}_i$ also

affect heat transfer. Moreover, it can be found that heat transfer will be enhanced by increasing $\overline{w}_o$ or decreasing $\overline{w}_i$. Consequently, the maximum heat transfer can be obtained at $\overline{w}_o$ = 0.97239 m/s and $\overline{w}_i$ = 0.11449 m/s according to the PEC based on the cases considered.

3. Although using non-Newtonian nanofluid as the working fluid may raise the pressure drop, the value of pressure drop is still less than the case of using water or Newtonian nanofluid as the working fluid. Besides, non-Newtonian nanofluid will achieve comparatively better heat transfer performance. In this paper, comparing with water, using non-Newtonian nanofluid (n = 0.5, ϕ = 5%, $\overline{w}_o$ = 0.97239 m/s) as the working fluid can lead to a heat transfer enhancement of 58-97% when $\overline{w}_i$ decreases from 0.23814 m/s to 0.11449 m/s. Also, the pressure drop reduces 36-45% from $\overline{w}_i$ = 0.11449 m/s to 0.23814 m/s. Despite the fact that ϕ = 5% results better $\overline{Nu}$, ϕ = 0% provides best performance in view of the PEC.

ACKNOWLEDGEMENT

The work was partially supported by the Ministry of Science and Technology Taiwan under the grant No. MOST-105-2221-E-006-094.

NOMENCLATURE

A	length of oval sections (mm)
A	cross-section inlet area of the outer pipe (mm^2)
B	length of transition sections (mm)
C	specific heat capacity (J kg^{-1} K^{-1})
d	diameter of the inner pipe circular sections (mm)
$d1$, $d2$	long and short diameter of the inner pipe oval sections (mm)
D	diameter of the outer circular pipe (mm)
D	diameter (mm)
D_h	hydraulic diameter (mm)
f, f_0	friction factor
F_1	blending function
$\tilde{G}_k$	generation of k equation (kg m^{-1} s^{-3})
G_ω	generation of ω equation (kg m^{-1} s^{-3})
h	convective heat transfer coefficient (W m^{-2} K^{-1})
k	thermal conductivity (W m^{-1} K^{-1})
k	turbulent kinetic energy (m^2 s^{-2})
K	flow consistency index (kg m^{-1} s^{-1})
L	length of circular sections (mm)
L	length (mm)
n	normal direction
$\overline{Nu}$, $\overline{Nu_0}$	average Nusselt number
$\overline{P}$	mean pressure (kg m^{-1} s^{-2})
P	pressure (kg m^{-1} s^{-2})
P	wetted perimeter of the cross-section of the outer pipe (mm)
Re	Reynolds number
t	thickness of the pipe walls (mm)
T	temperature (K)
$\overline{T}$	mean temperature (K)
u, v, w	velocity components (m s^{-1})
$\overline{u}_i$, $\overline{u}_j$	mean velocity in Einstein notation (m s^{-1})
u'_i, u'_j	turbulent velocity fluctuations in Einstein notation (m s^{-1})
U_{avg}	average velocity
V	velocity vector (m s^{-1})
x_i, x_j	Cartesian coordinate in Einstein notation (m)
z	flow direction

Greek symbols

σ_k	turbulent Prandtl number of k equation
σ_ω	turbulent Prandtl number of ω equation
$\sigma_{\omega,2}$	turbulent modeling constant
β^*	turbulent modeling constant
β	turbulent modeling constant
$\dot{\gamma}$	rate of shear strain (s^{-1})
ΔT_m	logarithmic mean temperature difference (LMTD)
μ	laminar dynamic viscosity (kg m^{-1} s^{-1})
μ_t	laminar dynamic viscosity (kg m^{-1} s^{-1})
ρ	density (kg m^{-3})
$\overline{\tau}_{ij}$	stress tensor (kg m^{-1} s^{-2})
ϕ	nanoparticle volume fraction
ω	specific dissipation rate (s^{-1})

Superscripts

n	flow behavior index

Subscripts

atm	atmospheric pressure
avg	average
bf	base fluid
ci	inlet of the cold pipe
co	outlet of the cold pipe
f	fluid
hi	inlet of the hot pipe
ho	outlet of the hot pipe
i	inlet of the inner pipe (hot pipe)
nf	non-Newtonian nanofluid

o	inlet of the outer pipe (cold pipe)
p	nanoparticle
s	solid
t	total

REFERENCES

Baheri Islami S, Dastvareh B, Gharraei R. “An investigation on the hydrodynamic and heat transfer of nanofluid flow with non-Newtonian base fluid in micromixers.” Int. J. of Heat and Mass Transfer 78 (2014) 917-29.

Chen WL, Fang LC. “A numerical study on the flow over a staggered oval tube for heat-transfer enhancement.” J. CSME. 25 (2004) 209-216.

Chen CK, Chen WL, Guo ZY. “A numerical study on the flow over a novel tube for heat-transfer enhancement with a linear eddy-viscosity model.” Int. J. of Heat and Mass Transfer 47 (14-16) (2004) 3431-3439.

Chen WL, Wong KD, Wong KL. “A parametric study on the laminar flow in an alternating horizontal or vertical oval cross-section pipe with computational fluid dynamics.” Int. J. of Heat and Mass Transfer 49 (2006) 287-296.

Chen WL. “A numerical study on the heat-transfer characteristics of an array of alternating horizontal or vertical oval cross-section pipes placed in a cross stream.” Int. J. Refrigeration 30 (2007) 454-463.

Chen WL, Dung WC. “Numerical study on heat transfer characteristics of double tube heat exchangers with alternating horizontal or vertical oval cross section pipes as inner tubes.” Energy Conversion and Management 49 (2008) 1574-1583.

Guo ZY. “A brief introduction to a novel heat-transfer enhancement heat exchanger.” Internal report (2003) Department of EMEMKLEHTEC, Tsinghua University, Beijing, China.

Bagheri R, Gh. Etemad S, Hojjat M. “Laminar heat transfer of non-Newtonian nanofluids in a circular tube.” Korean J. Chemical Engineering 27 (2010) 1391-1396.

Bagheri R, Gh. Etemad S, Hojjat M, Thibault J. “Convective heat transfer of non- Newtonian nanofluids through a uniformly heated circular tube.” Int. J. Thermal Sciences 50 (4) (2010) 525-531.

Kang HU, Kim SH, Oh JM. “Estimation of thermal conductivity of nanofluid using experimental effective particle volume.” Exp. Heat Transfer 19 (3) (2006) 181-191.

Lamraoui H, Mansouri K, Saci R. “Numerical investigation on fluid dynamic and thermal behavior of a non-Newtonian Al_2O_3-water nanofluid flow in a confined impinging slot jet.” J. non-Newtonian fluid mechanics 265 (2019) 11-17.

Feng B, He YL, Li B, Tao WQ. “Experimental study on friction factor and numerical simulation on flow and heat transfer in an alternating elliptical axis tube.” Applied Thermal Engineering, 26 (17) (2006) 2336-2344.

Al-Nimr MA, Kianifar A, Kleinstreuer C, Mahian O, Pop I, Sahin AZ et al. “A review of entropy generation in nanofluid flow.” Int. J. of Heat and Mass Transfer 65 (2013) 514-532.

Chen ZJ, Li ZX, Liang XG, Meng JA. “Experimental study on convective heat transfer in alternating elliptical axis tubes.” Experimental Thermal and Fluid Science 29 (4) (2005) 457-465.

Menter FR. “Zonal two-equation k-ω turbulence models for aerodynamic flows.” AIAA-Paper No 93-2906 (1993).

Menter FR. “Two-equation eddy-viscosity turbulence models for engineering applications.” AIAA J. 32 (8) (1994) 1598-1605.

Najafi Khaboshan H, Nazif HR. “Heat transfer enhancement and entropy generation analysis of Al_2O_3-water nanofluid in an alternating oval cross-section tube using two-phase mixture model under turbulent flow.” Int. J. of Heat and Mass Transfe 54 (2018) 3171-3183.

Najafi Khaboshan H, Nazif HR. “Entropy generation analysis of convective turbulent flow in alternating elliptical axis tubes with different angles between pitches; a numerical investigation.” Int. J. of Heat and Mass Transfer 55 (2019) 2857-2872.

Hanafizadeh P, Karbalaee MS, Vaezi S. “Effect of aspect ratio on heat transfer enhancement in alternating oval double pipe heat exchangers.” Applied Thermal Engineering 125 (2017) 1164-1172.

Kim NH, Webb RL. Principles of enhanced heat transfer, 2nd ed., Taylor & Francis; New York, 2005.

Chen L, Wu Q, Xie H. “Measurements of the viscosity of suspensions (nanofluids) containing nanosized Al_2O_3 particles.” High Temp.-High Pressures 37(2) (2008) 127-135.

非牛頓奈米流體在交叉橢圓套管中熱交換之數值模擬研究

林晨興　陳朝光
國立成功大學機械工程學系

陳介力
國立成功大學航空太空工程學系

摘 要

本研究藉數值模擬的方法，研究分別以非牛頓奈米流體與水作為交叉橢圓管套管內管及外管部分的工作流體時，所發生的熱交換行為。非牛頓奈米流體係以非牛頓流體為基液，掺入金屬或金屬氧化物的奈米粒子而成。本篇研究假設非牛頓奈米流體為單相流液體，探討在不同的流動特性指數、內管和外管入口初速、奈米體積分率時的熱交換行為。故此，文中計算並分析了溫度場、流場、壓降、場協同角、平均紐賽數及 PEC。結果顯示，若要提升熱傳效果，可藉由降低流動特性指數、降低內管初速、增加外管初速及減少奈米體積分率來達成。